J. Meas. Sci. Instrum., 2025, 16(4): 603-611.
DOI: 10.62756/jmsi.1674-8042.2025058
http://jmsi.publish.founderss.cn/
jmsi@nuc.edu.cn

Metamaterial pressure sensor based on ceramic for harsh environments

FENG Rui[1,2*], QIAO Yi[1,2], WU Dongyang[1,2], TAN Shijian[1,2], TAN Qiulin[1,2]

1. State key Laboratory of Extreme Environment Optoelectronic Dynamic Measurement Technology and Instrument, North University of China, Taiyuan 030051, China;
2. Key Laboratory of Micro/Nano Devices and Systems, Ministry of Education, North University of China, Taiyuan 030051, China

***Corresponding author:** FENG Rui (ruifeng@nuc.edu.cn)

Received: September 11, 2025 **Revised:** October 29, 2025 **Accepted:** November 23, 2025

Abstract: This paper presents a new type of ultra-material microwave pressure sensor designed for extreme environments, and conducts a systematic study on its structural design, manufacturing process, working mechanism, and experimental performance. The sensor is based on the cross-slot ultra-material resonant structure. Platinum-based conductive patterns are precisely fabricated on a high-purity alumina ceramic substrate through screen printing, and a strong bond between metal and ceramic is achieved through high-temperature sintering. Thanks to the high-temperature stability of the ceramic material and the high precision of the process, this sensor maintains excellent structural integrity and performance consistency in harsh environments. The working mechanism of the sensor is based on the microstructural deformation induced by pressure. When external pressure is applied to the ceramic cavity, the deformation of the cavity will change the equivalent electromagnetic boundary conditions inside, thereby causing perturbations in the resonant modes of the metamaterial, resulting in a continuous measurable shift in the resonant frequency. Based on this mechanism, the change in pressure can be precisely mapped to the frequency change, enabling wireless and passive pressure measurement. By utilizing the intrinsic resonant radiation of the metamaterial to achieve coupled readings, the complexity of sensor integration is significantly reduced and its working reliability in high-pressure, high-temperature, and strong electromagnetic interference environments is improved. During the design stage, the influence laws of the geometric parameters of the metamaterial and other factors on the resonant performance and pressure sensitivity were analyzed through finite element coupling simulation. Experimental verification shows that the sensor exhibits excellent linear pressure response within the range of 0—500 kPa, and maintains good repeatability and frequency stability in the high-pressure zone. The maximum sensitivity reaches 135 kHz/kPa, and the frequency drift is minimal during multiple loading-unloading cycles, fully demonstrating that the structural strength and reliability of the design meet the engineering requirements. The sensor proposed in this study could achieve long-term stable operation in aerospace engine compartments, high-temperature metallurgical furnaces, deep mine pressure monitoring, petrochemical high-corrosion pipelines, and extreme environment equipment. This research not only demonstrated the potential of integrating metamaterials with advanced ceramic processes to construct wireless passive sensors, but also provided new design ideas and process routes for the engineering application of microwave sensing technology in harsh environments.

Key words: pressure sensor; wireless passive; high-temperature co-fired ceramic; ceramic process; microwave; aerospace and aviatio

0 Introduction

In high-risk manufacturing and transportation tasks, various unexpected failures and environmental hazards often lead to significant economic losses and human resource waste. Pressure measurement[1-3] holds significant importance in those fields, such as aerospace[4,5], mining and metallurgy[6], and so on. During the operation of aerospace crafts, their surfaces, engines, and gas turbines are typically subjected to harsh conditions such as high temperatures and pressures. Thus, it is crucial to accurately obtain real-time pressure parameters, which serve as the foundation and guarantee for material selection, structural design, and protective formulation of aerospace vehicles. The traditional wired measurements[7,8] are prone to electric sparks and cannot be used safely in confined spaces, restricting their application in harsh environments.

In response to these pressing technological challenges, the wireless passive sensor is designed for real-time monitoring of key parameters in severe environments. Those sensors can achieve non-contact pressure sensing by remotely detecting shifts in their resonant frequency, thereby providing essential data for system operation and supporting intelligent functions such as fault prediction, structural adjustment, and maintenance decision-making.

Various sensing working mechanisms have been applied for wireless sensors, including LC resonance[9-13], surface acoustic wave (SAW) [14-17], and microwave scattering techniques[18-22]. The surface acoustic wave pressure sensor realizes wireless pressure detection by the change of surface acoustic waves in piezoelectric materials after sensing external actions. However, the piezoelectric materials inside such sensors may limit their applications, suffering from serious electrical loss, poor stability, and complex preparation processes. The LC resonant pressure sensor is typically composed of a sensing capacitor combined with a planar spiral inductor to form an LC resonant circuit. With the change of the measured parameters, the capacitor responds accordingly, thereby causing changes in the relevant parameters of the LC resonant circuit. Limited by the LC resonance principle, LC sensors usually have a short detection distance, and their signals are prone to attenuation or distortion due to environmental factors such as metal objects and electromagnetic interference. Moreover, they have relatively low measurement accuracy, making it difficult to meet the requirements of high-precision detection scenarios. Microwave scattering-based sensors have the advantages of compact form factor, low-mass design, robust remote sensing capabilities, and fine-grained frequency resolution, which endow them with the requisite performance attributes for precise measurement of physical quantities, such as temperature[23-25], pressure[26-29], strain[30-32], and so on[33,34].

In this work, we designed and implemented a prototype of a wireless passive metamaterial-based microwave pressure sensor relying on the microwave scattering mechanism, targeting pressure parameter detection in harsh environments. By analyzing the propagation behavior of electromagnetic waves within resonant structures and their response mechanisms to external pressure changes, the operating principle of the sensor was systematically elucidated. High-frequency electromagnetic simulation tools were used to model and optimize the metamaterial unit, investigating the influence of geometric parameter variations on resonant frequency, and simulating pressure loading scenarios representative of actual working environments. Subsequently, a rigid sensor sample was fabricated using HTCC (High-temperature co-fired ceramic) technology, employing alumina ceramic as the substrate and platinum as the conductive layer. An experimental measurement platform was then constructed to validate its performance. The results showed that the sensor had excellent frequency stability and sensitivity across a pressure range of 0 — 500 kPa. The resonant frequency exhibited a linear shift with varying external pressure, confirming the feasibility and engineering potential of this structure for non-contact, real-time pressure monitoring in high-pressure environments.

1 Theoretical analysis

The schematic of the pressure sensor is shown in Fig.1 (a). And the surface and bottom patterns of the sensor are shown in Fig.1 (b). The blue part is the platinum metal section, and the grey part is the alumina ceramic. The platinum is selected as the conductive material for the top and bottom layers, and the alumina ceramic with a total height of 1 mm is used as the dielectric substrate, ensuring long-term stable operation of the device under harsh conditions such as high pressure. A sealed cavity is fabricated in the center of the alumina ceramic with a height of 0.6 mm between the metallic layers.

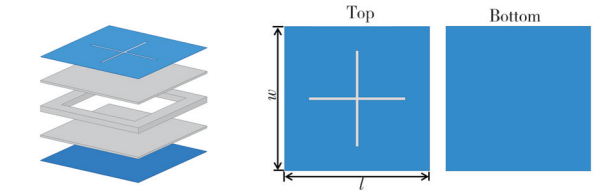

(a) Schematic of pressure sensor (b) Top and bottom views of pressure sensor

Fig. 1 Structure of pressure sensor

The schematic of the wireless transmission mechanism and the metamaterial-based pressure sensor is presented in Fig. 2. The coplanar waveguide (CPW) antenna used as an interrogation antenna emits an excitation signal to the pressure sensor. When the transmitted frequency is identical to the self-resonant frequency of the pressure sensor, specific electromagnetic waves induce continuous oscillations within the cross-groove metamaterial resonator. The pressure sensor reflects other frequencies back to the interrogation antenna, as the matched frequency component decays over time in the metamaterial resonator. The resonant frequency of the pressure sensor is extracted from the measured S_{11} parameter, and the pressure parameters are deduced through the shift of the resonant frequency in S_{11}.

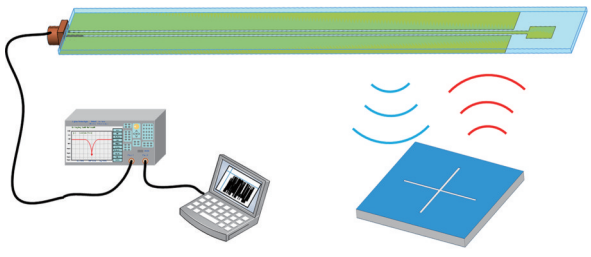

Fig. 2 Wireless sensing mechanism of metamaterial-based pressure sensor

1.1 Principle of metamaterial pressure sensor

Compared to a surface acoustic wave (SAW) -type pressure sensor composed of an antenna and a sensitive structure for the pressure parameter. The proposed metamaterial sensor integrates the antenna and sensing functions, eliminating the need for a discrete signal transmission antenna. This is typically achieved by introducing a cross-groove metamaterial structure onto the top layer to precisely manipulate the propagation characteristics of electromagnetic waves. The designed metamaterial pressure sensor employs a resonant unit based on the cross-groove structure, incorporating a miniature cavity beneath it.

The underlying principle of this wireless transmission and sensing mechanism can be analogized to the resonant circuit model illustrated in Fig.3, where the metamaterial structure functions as an equivalent resonator. Its resonant frequency shifts in response to applied external pressure. In general, a microwave resonator can be equivalent to an RLC circuit, and its resonant frequency is determined by

$$f=\frac{1}{2\pi\sqrt{LC}}, \tag{1}$$

where f denotes the resonant frequency of the pressure sensor, L and C signify the equivalent inductance and capacitance of the pressure sensor, respectively. The equivalent capacitance C can be decomposed into two fundamental components: the interlayer coupling capacitance between the upper and lower metallic interfaces (C_i) arising from electromagnetic interaction, and the structural capacitance of the cross-groove metamaterial configuration (C_g) determined by its geometric topology. This decomposition is mathematically formulated as

$$C=C_i+C_g. \tag{2}$$

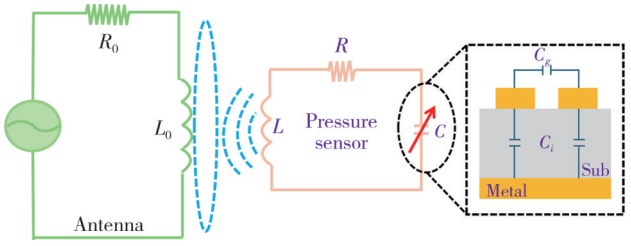

Fig. 3 Schematic and circuit model of metamaterial-based pressure sensor

An embedded sealed cavity within the pressure sensor serves as the pressure-sensing element. When ambient air pressure is applied to the cavity, deformation of the cavity causes the distance d between the upper and lower metallic surfaces to vary. This variation in spacing induces a change in the coupling capacitance C_i between the metal surfaces, thereby leading to a shift in the resonant frequency of the pressure sensor. According to the definitions of the bending stiffness and the central deflection of the thin plate, the distance d under applied pressure is characterized by[35]

$$d=\frac{Pa^4}{64w}. \tag{3}$$

Then w can be expressed as

$$w=\frac{Et^3}{12(1-v^2)}. \tag{4}$$

Ultimately, the distance between the upper and lower ends of the sensor's cavity can be expressed as

$$d=\frac{3Pa^4(1-v^2)}{16Et^3}, \tag{5}$$

where v and E denote the Poisson's ratio and Young's modulus of the substrate, respectively, P signifies the applied pressure, a represents the side length of the square capacitor patch, and t denotes the thickness of the sensitive film. The corresponding capacitance is given by

$$C_i=\frac{\varepsilon_r\varepsilon_0 A}{x}, \tag{6}$$

where ε_0 denotes the permittivity of free space and ε_r represents the relative permittivity of the substrate material, A signifies the overlapping area of the capacitor plates, and x denotes the separation distance between the upper and lower capacitor electrodes.

The core physical principle of the sensor lies in the fact that cavity deformation alters the thickness or internal gap of the resonant cavity structure, leading to changes in the equivalent capacitance C, and thereby shifting the resonant frequency f. By analyzing the frequency response changes of the reflection coefficient S_{11} under varying pressures, quantitative evaluation of the applied pressure can be realized.

Fig.4 illustrates the simulated S_{11} variation with different surface lengths in the x- and y-directions. The optimal dimensions of the sensing patch are finally determined as x=0.25 mm and y=8 mm, where the sensor exhibits stable resonance and good impedance matching.

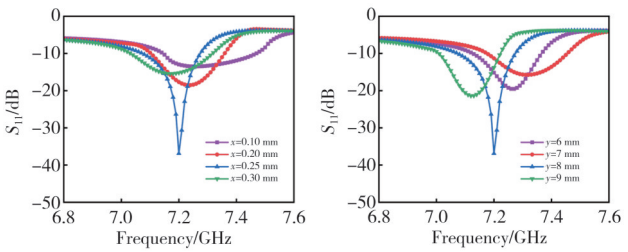

(a) Curve of pressure sensor with respect to change of x (b) Curve of pressure sensor with respect to change of y

Fig. 4 Optimization of structure of pressure sensor

1.2 Principle of coplanar waveguide antenna

For the coplanar waveguide (CPW) antenna as displayed in Fig.5(a), a series of iterative simulations and optimizations are systematically performed to determine its optimal structural parameters, as comprehensively summarized in Table 1.

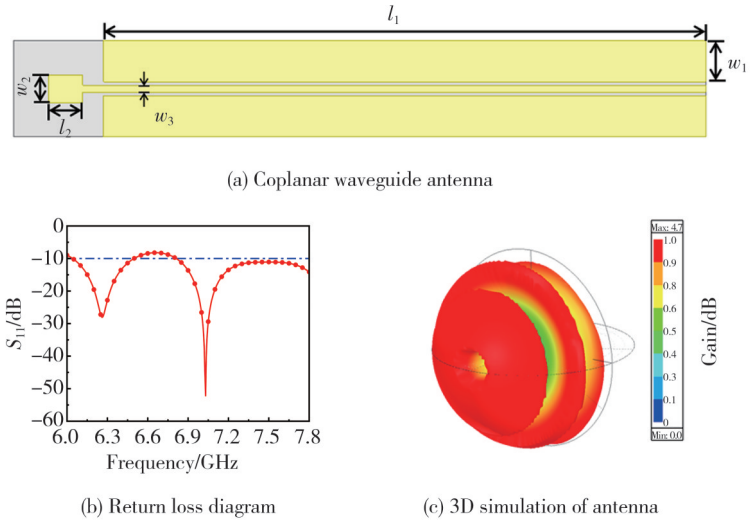

(a) Coplanar waveguide antenna

(b) Return loss diagram

(c) 3D simulation of antenna

Fig. 5 Coplanar waveguide antenna

Table 1 Sensor and CPW antenna size

Parameter	Value/mm
x	0.25
y	8
w	12
l	12
w_1	5.5
l_1	87
w_2	4.7
l_2	7
w_3	0.5

The optimized reflection coefficient S_{11} of the CPW antenna, depicted in Fig.5(b), demonstrates outstanding impedance matching performance within the 6.8—8 GHz frequency spectrum. Notably, the S11 values remain well below the critical threshold of —10 dB throughout this frequency band, which signifies superior electromagnetic energy coupling efficiency for both reception and transmission processes. Such exceptional performance ensures that the CPW antenna can reliably facilitate the stable operation of the microwave-based sensor system, thereby enabling accurate and consistent sensing functionality.

Fig.5(c) depicts the three-dimensional radiation pattern of the antenna, comprehensively characterizing its radiation attributes, including the main lobe orientation and gain distribution. The radiation gain of the CPW antenna is 4.7 dB along the main lobe direction, which underscores its exceptional directivity and energy focusing capability. This feature renders the antenna particularly well-suited for microwave sensing systems demanding a high signal-to-noise ratio, enabling efficient signal acquisition and processing in complex electromagnetic environments.

The radiation pattern demonstrates an excellent overall symmetry, indicating balanced radiation performance across all directions and stable directional consistency. This characteristic is crucial for guaranteeing robust signal transmission and long-term operational stability of the pressure sensor system, which is of practical applicability as both an excitation and receiving element in harsh environmental scenarios.

To evaluate the effect of the interrogation distance on the wireless coupling characteristics, HFSS simulations were conducted with different separations between the sensing unit and the interrogation antenna. As illustrated in Fig. 6, the resonant of the sensor can still be clearly observed under all simulated distances, demonstrating stable electromagnetic coupling.

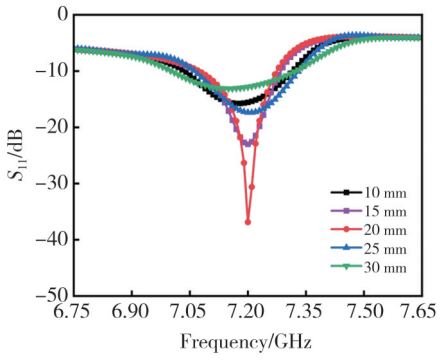

Fig. 6 Relationship between distance between antenna and sensor and S11

With the increase in distance, the depth of the S_{11} notch becomes shallower and the Q-factor slightly decreases, which is attributed to the weakened near-field coupling strength and additional propagation loss. Considering both coupling efficiency and structural integration requirements, the final interrogation distance was optimized and fixed at 20 mm in subsequent experiments and measurements.

1.3 Simulation of pressure sensor

To evaluate the structural stability of the sensor under external pressure and its impact on electromagnetic response performance, COMSOL multiphysics is utilized to conduct multiphysics simulation analysis of the stress and deformation distribution of the sensor under various pressure loads. The corresponding simulation is illustrated in Fig. 7(a), which demonstrates that across a pressure span of 0 — 500 kPa, the stress at the location of peak deformation persists well beneath the material's yield threshold. This observation substantiates the sensor's superior structural soundness when subjected to high-pressure regimes.

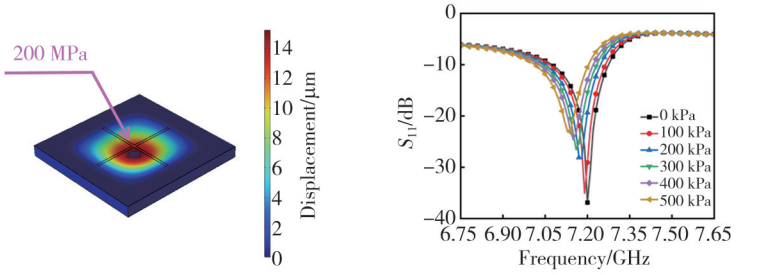

(a) Stress simulation diagram (b) Simulation results of pressure sensor

Fig. 7 Performance simulation of pressure sensors

To further investigate the effect of cavity compression on the resonant frequency, the geometrical variation parameters obtained from the COMSOL simulations were imported into ANSYS HFSS to construct equivalent geometrical models corresponding to different pressure states for electromagnetic simulation analysis.

In the HFSS simulation, we set the radiation boundary condition on the outer surface of the model and used the wave port to excite the coplanar waveguide feed line. The base material was selected as HTCC aluminum oxide ceramic, with a relative dielectric constant of 9.8 and a dielectric loss tangent of 0.002 at room temperature, which was a high-stiffness ceramic material. To ensure the convergence and accuracy of the simulation results, we set the maximum number of iterations to 30.

As shown in Fig. 7(b), the simulation results demonstrate a consistent shift in the sensor's resonant frequency with increasing applied pressure. Moreover, a strong correlation is observed between the frequency shift and the deformation height of the cavity, confirming the sensor's pressure-sensitive resonance behavior.

2 Processing of sensor and antenna

The fabrication process of the proposed pressure sensor is illustrated in Fig. 8(a). The sensor adopts high-temperature co-fired ceramic (HTCC) alumina with 99% purity as the substrate material, which offers excellent corrosion resistance. The manufacturing process mainly involves key steps such as punching, lamination, sintering, and screen printing. First, the intermediate ceramic layers of the sensor are processed using a punching machine to create a cavity for pressure sensing. Then the carbon films are filled in the square cavity.

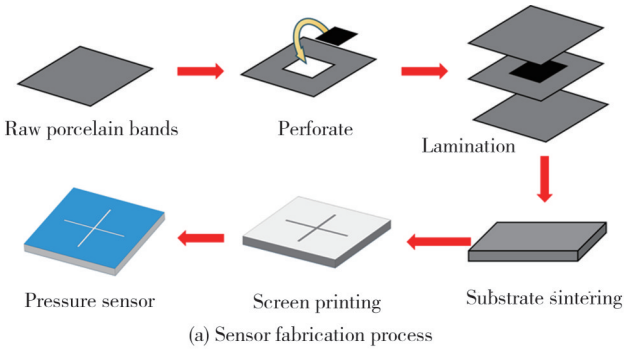

(a) Sensor fabrication process

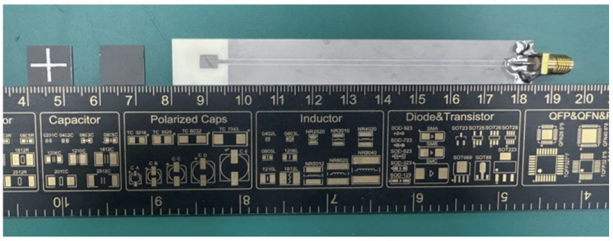

(b) Pressure sensor and CPW antenna

Fig. 8 Manufacturing process of pressure sensor

During the lamination stage, to improve the density of the green ceramic tapes, all the layers of the sensor with an embedded cavity filled with carbon films are first encapsulated in a vacuum-sealed bag. Air is evacuated using a vacuum system to avoid gas entrapment, which could cause structural porosity during lamination. The sealed tapes are then subjected to hot isostatic pressing in

warm water at 70 ℃ and 20 MPa for 20 min. This step activates the binder and enhances inter-particle bonding among the alumina grains, forming a compact and uniform layered structure.

Following the lamination process, the sensor undergoes high temperature sintering to enhance the mechanical strength of the substrate and induce robust chemical bonding between the green ceramic layers. Considering the thermal shrinkage of alumina during sintering, particularly in the x and y directions, dimensional compensation is applied based on the material's actual shrinkage rate to ensure final dimensional accuracy.

The pressure sensors are then placed in a muffle furnace and sintered at a final temperature of 1 570 ℃. During the temperature ramp-up to 600—700 ℃, atmospheric oxygen reacts with the carbon films, generating carbon dioxide (CO_2) that escapes through the porous structure of the unsintered green tapes. Simultaneously, ambient air infiltrates the cavity to equalize internal pressure. To safeguard the integrity of the sensitive membrane, a 300-minute holding period is implemented at this temperature range to ensure complete combustion of the carbon films, thereby facilitating the formation of a hermetically sealed cavity. This high-temperature process densifies the alumina particles and transforms the green body into a mature ceramic structure with high hardness and thermal resistance.

Platinum exhibits excellent oxidation resistance, corrosion resistance, and long-term electrical stability under harsh environments such as high pressure and chemically aggressive atmospheres. In contrast, silver tends to suffer from electromigration and corrosion, while gold—although chemically stable—has significantly higher cost and lower mechanical robustness, making it less suitable for long-duration stress-bearing applications. Alumina ceramic possesses high mechanical strength, hermeticity, and superior dielectric insulation, enabling the structure to withstand large external pressure loads. Moreover, it is fully compatible with the HTCC co-firing process, ensuring reliable and integrated device packaging. Therefore, despite higher material cost and fabrication complexity, the combination of platinum and alumina provides the most reliable solution for robust and long-term pressure sensing in harsh conditions.

The metallized patterns on the top and bottom of the pressure sensor were formed with platinum paste by screen printing technology. The post-sintering of the surface metal layer of the sensor is carried out with peak temperatures exceeding 1 200 ℃ for extended durations. The post-sintering process facilitated the volatilization of organic solvents and bonding additives in the platinum paste, ensuring the formation of a stable platinum metal film on the ceramic surface. The resulting ceramic substrate exhibits excellent mechanical and thermal stability, ensuring reliable sensor operation under extreme conditions. The photographs of the finalized sensor and CPW antenna are presented in Fig.8 (b).

3 Experiment

To evaluate the performance of the fabricated pressure sensor, a dedicated testing platform is established, as illustrated in Fig.9.

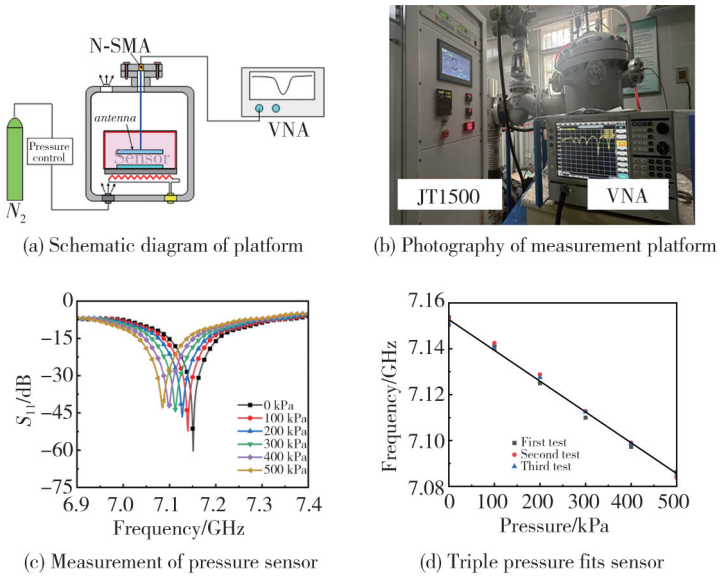

(a) Schematic diagram of platform (b) Photography of measurement platform

(c) Measurement of pressure sensor (d) Triple pressure fits sensor

Fig. 9 Performance testing of pressure sensors

The system primarily consists of a pressure furnace, a vector network analyzer (VNA), a computer, and an S-type standard pressure gauge. The pressure furnace provides a controlled pressure environment, with the

pressure level adjusted and monitored through an external control panel, while the VNA is employed to acquire the sensor's electromagnetic response.

Before the S-parameter measurements, a one-port SOLT (Short-open-load-thru) calibration was performed on the vector network analyzer (VNA). During the calibration, the test fixture was properly mounted, and the standard short, open, and matched-load elements were sequentially connected to eliminate systematic errors. The calibration accuracy was validated by re-measuring the standard load to ensure consistency with theoretical reflection characteristics.

To evaluate the reliability of the measured resonant frequency shift, a comprehensive uncertainty analysis was performed by considering the contributions from instrumentation error, environmental fluctuation, and repeatability of measurements. The uncertainty introduced by the VNA was obtained from the manufacturer's specifications, which was estimated to be ±5 MHz. In addition, a pressure furnace with argon gas loading was used to apply the external pressure, and the pressure measurement uncertainty was maintained within ±5 kPa throughout the experiments. During measurement, the ambient temperature was controlled at 25 ℃, and the temperature variation was limited within ±5 ℃, effectively minimizing the influence of thermal drift on the resonant frequency.

The pressure testing is conducted by configuring the furnace to follow a pressurization sequence using externally supplied argon gas. Pressurization is incremented in 100 kPa steps, with measurements taken after each step. At each stage, the S11 data of the sensor is recorded until the pressure reaches 500 kPa. The corresponding resonant curves of the sensor across the 0 — 500 kPa range are shown in Fig. 9(c). The results demonstrate that the sensor has excellent sensitivity to pressure variations, with its resonant frequency shifting downward from 7.153 75 GHz to 7.086 25 GHz as pressure increased, amounting to a total shift of 0.067 5 GHz. This trend is consistent with the operating principle of the pressure sensor.

The sensitivity of the sensor is determined to be approximately 135 kHz/kPa through the extraction of resonant frequency points from the measured S11 curves. Following the release of pressure and its return to atmospheric conditions, three independent measurement trials are conducted to assess repeatability. As presented in Fig. 9(d), the resonant frequency responses across the three trials exhibit significant consistency, with frequency deviations maintained within ±0.01 GHz. The nearly linear relationship between pressure and resonant frequency confirms the sensor possesses the capability for accurate, repeatable, and reliable pressure monitoring under harsh environmental conditions.

The comparison results of this study with recent pressure sensors are shown in Table 2. This scheme demonstrates great potential in terms of sensitivity and practicality.

Table 2 Sensor and CPW antenna size

Method	Size/mm^2	Sensitive/(kHz•kPa^{-1})	Range/kPa
Ref.[26]	75×14	6.31	350
Ref.[27]	95×58	3.51	440
Ref.[28]	20×20	139.7	300
This work	12×12	135	500

4 Conclusions

This paper presents a metamaterial-based microwave wireless passive pressure sensor engineered for precise pressure monitoring in extreme environments. Leveraging high-temperature co-fired ceramic (HTCC) as the substrate and a platinum conductive layer, the sensor ensures exceptional structural stability and chemical resistance, critical for harsh operational conditions. The integration of a sealed cavity within the sensor structure enables pressure-induced modulation of the metamaterial resonator, facilitating high-sensitivity non-contact sensing through linear shifts in microwave resonant frequency. Experimental validation confirms the sensor demonstrates a linear frequency response across 0—500 kPa, achieving a sensitivity of 135 kHz/kPa. This design addresses key limitations of traditional sensing technologies, offering robust wireless passive operation for aerospace, energy transportation, and metallurgical applications. The research not only provides a reliable solution for harsh-environment sensing but also paves the way for developing integrated multi-parameter sensing systems through its modular metamaterial architecture.

Although the present study experimentally verified the feasibility and high sensitivity of the proposed HTCC-based passive pressure sensor, the measurement setup was conducted under ideal laboratory conditions using an external vector network analyzer (VNA). In practical applications, metallic mounting structures and surrounding components may introduce additional detuning or signal attenuation, which were not considered in this work.

Future research will therefore focus on improving environmental adaptability and system integration. Specifically, electromagnetic shielding and impedance-matching techniques will be investigated to mitigate the

influence of metallic surroundings. Furthermore, a miniaturized, low-cost wireless interrogation module will be developed to replace the VNA, enabling real-time, portable, and low-power operation in industrial and aerospace environments. These efforts will further enhance the practicality and scalability of the proposed sensing system.

Acknowledgement

This work was supported by Key Research and Development Plan of Shanxi Province (Nos. 202102030201005, 202203021222022), National Natural Science Foundation of China (No. 62401522), Fundamental Research of Shanxi Province (No. 202203021222070), China Postdoctoral Science Foundation (No. 2023M743313), Research Project Supported by Shanxi Scholarship Council of China.

Declaration of conflicting interests

The authors have no conflicts of interest related to the content of this article.

References

[1] HU M W, CHEN P D, QU X C, et al. Theoretical and experimental investigation on performance enhancement effect for a novel capacitive pressure sensor with double-cavity. IEICE Electronics Express, 2023, 20(13): 20230187.

[2] XIONG J J, WU G Z, TAN Q L, et al. Dielectrically-loaded cylindrical resonator-based wireless passive high-temperature sensor. Sensors, 2016, 16(12): 2037.

[3] KAKEHI Y, YAMADA Y, KONDO Y, et al. Electrical and piezoresistive properties of titanium oxycarbide thin films for high-temperature pressure sensors. Vacuum, 2021, 193: 110550.

[4] MOSER M, PRADHAN M, ALOMARI M, et al. Model and simulation of GaN-based pressure sensors for high temperature applications: part I: physics based compact modeling. IEEE Sensors Journal, 2021, 21(18): 20165-20175.

[5] JAVED Y, MANSOOR M, ALI SHAH I. A review of principles of MEMS pressure sensing with its aerospace applications. Sensor Review, 2019, 39(5): 652-664.

[6] SHAO Z Q, WU Y L, WANG S, et al. All-sapphire-based fiber-optic pressure sensor for high-temperature applications based on wet etching. Optics Express, 2021, 29(3): 4139-4146.

[7] CHEN Z F, WANG Z, LI X M, et al. Flexible piezoelectric-induced pressure sensors for static measurements based on nanowires/graphene heterostructures. ACS Nano, 2017, 11(5): 4507-4513.

[8] MANNSFELD S C B, TEE B C, STOLTENBERG R M, et al. Highly sensitive flexible pressure sensors with microstructured rubber dielectric layers. Nature Materials, 2010, 9(10): 859-864.

[9] WANG Y, TAN Q L, ZHANG L, et al. Wireless passive LC temperature and strain dual-parameter sensor. Micromachines, 2021, 12(1): 34.

[10] MA M S, WANG Y, LIU F, et al. Passive wireless LC proximity sensor based on LTCC technology. Sensors, 2019, 19(5): 1110.

[11] FONSECA M A, ENGLISH J M, VON ARX M, et al. Wireless micromachined ceramic pressure sensor for high-temperature applications. Journal of Microelectromechanical Systems, 2002, 11(4): 337-343.

[12] TAN Q L, LU F, JI Y H, et al. LC temperature-pressure sensor based on HTCC with temperature compensation algorithm for extreme 1100 ℃ applications. Sensors and Actuators A: Physical, 2018, 280: 437-446.

[13] TAN Q L, LUO T, WEI T Y, et al. A wireless passive pressure and temperature sensor *via* a dual LC resonant circuit in harsh environments. Journal of Microelectromechanical Systems, 2017, 26(2): 351-356.

[14] MEMON M M, LIU Q, MANTHAR A, et al. Surface acoustic wave humidity sensor: a review. Micromachines, 2023, 14(5): 945.

[15] OKUDA S, ONO T, KANAI Y, et al. Graphene surface acoustic wave sensor for simultaneous detection of charge and mass. ACS Sensors, 2018, 3(1): 200-204.

[16] PAN Y, YAN C C, GAO X, et al. A passive wireless surface acoustic wave (SAW) sensor system for detecting warfare agents based on fluoroalcohol polysiloxane film. Microsystems & Nanoengineering, 2024, 10: 4.

[17] ZHANG H, MU D Y, ZHANG Z C, et al. Surface acoustic wave sensors for wireless temperature measurements above 1200 degree Celsius. Sensors, 2024, 24(15): 4945.

[18] LIU Y F, CHEN Y, LI J, et al. Terahertz biaxial strain sensor based on double-upright cross metamaterial. Micromachines, 2023, 14(4): 816.

[19] SHAHZAD W, HU W D, ALI Q, et al. A low-cost metamaterial sensor based on DS-CSRR for material characterization applications. Sensors, 2022, 22(5): 2000.

[20] SU S J, LU F, WU G Z, et al. Slot antenna integrated re-entrant resonator based wireless pressure sensor for high-temperature applications. Sensors, 2017, 17(9): 1963.

[21] LIU C J, LIAO C W, PENG Y J, et al. Microwave sensors and their applications in permittivity measurement. Sensors, 2024, 24(23): 7696.

[22] LI B, SHEN J W, HAN H Y, et al. Design and 3-D printing-assisted fabrication of microwave resonator-based passive wireless sensors for simultaneous measuring high temperatures and pressures. IEEE Sensors Journal, 2024, 24(17): 27205-27217.

[23] KOU H R, YANG L B, ZHANG X Y, et al. Wireless passive microwave antenna-integrated temperature sensor based on CSRR. Micromachines, 2022, 13(4): 621.

[24] SHI N Y, ZHANG L, FENG R, et al. CSRR-SIW

wireless passive high quality factor temperature sensor. IEICE Electronics Express, 2024, 21(14): 20240241.
[25] ZHANG X X, FENG R, HOU Y L, et al. Metamaterial high-temperature sensor based on all-planar substrate integrated waveguide. IEEE Sensors Journal, 2024, 24(7): 9916-9924.
[26] ZHU C, TANG Y, GUO J, et al. High-temperature and high-sensitivity pressure sensors based on microwave resonators. IEEE Sensors Journal, 2021, 21(17): 18781-18792.
[27] ZHANG Y Q, SHAFIEI M, WEN J Z, et al. Simultaneous detection of pressure and bending using a microwave sensor with tag and reader structure. IEEE Transactions on Instrumentation and Measurement, 2023, 72: 9511311.
[28] YANG L B, KOU H R, WANG X L, et al. A microwave pressure sensor loaded with complementary split ring resonator for high-temperature applications. Micromachines, 2023, 14(3): 635.
[29] FAN J X, LI X E. Dynamic calibration method of capacitive pressure measuring device. Journal of Measurement Science and Instrumentation, 2013, 4(1): 1-5.
[30] BAGHELANI M, ABBASI Z, DANESHMAND M. High-dynamic-range chipless microwave resonator-based strain sensor. IEEE Transactions on Instrumentation and Measurement, 2021, 70: 8003207.
[31] TANG Y, CHEN Y Z, ZHANG Q, et al. Enhanced sensitivity and robustness in an embeddable strain sensor using microwave resonators. IEEE Transactions on Instrumentation and Measurement, 2024, 73: 8003208.
[32] PENG H J, YANG X Q, SU P Q, et al. A noncontact feed microwave metal devices deformation and stress sensor based on metamaterial. IEEE Transactions on Industrial Electronics, 2023, 70(9): 9642-9652.
[33] MIAN M U, DENNIS J O, KHIR M H M, et al. Experimental analysis of out-of-plane Lorentz force actuated magnetic field sensor. IEICE Electronics Express, 2017, 14(5): 20161257.
[34] RIPKA P, JANOSEK M. Advances in magnetic field sensors. IEEE Sensors Journal, 2010, 10(6): 1108-1116.
[35] KOU H R, TAN Q L, WANG Y, et al. A wireless slot-antenna integrated temperature-pressure-humidity sensor loaded with CSRR for harsh-environment applications. Sensors and Actuators B: Chemical, 2020, 311: 127907.

基于陶瓷的适用于恶劣环境的超材料压力传感器

冯　瑞[1,2*], 乔　奕[1,2], 吴东洋[1,2], 谭世坚[1,2], 谭秋林[1,2]

1. 中北大学 极端环境光电动态测量技术与仪器国家重点实验室, 山西 太原 030051;
2. 中北大学 教育部微纳器件与系统重点实验室, 山西 太原 030051

摘　要： 本文介绍了一种专为极端环境设计的新型超材料微波压力传感器，并对其结构设计、制造工艺、工作原理及实验性能进行了系统研究。该传感器基于交叉槽超材料谐振结构。通过丝网印刷技术，在高纯度氧化铝陶瓷基板上精确制造出铂基导电图案，并通过高温烧结实现金属与陶瓷之间的牢固结合。由于陶瓷材料的高温稳定性以及工艺的高精度，该传感器在恶劣环境中仍能保持出色的结构完整性和性能一致性。该传感器的工作原理是基于压力引起的微观结构变形。当外部压力作用于陶瓷腔体时，腔体的变形会改变内部的等效电磁边界条件，从而导致超材料谐振模式的扰动，进而引起谐振频率的连续可测量变化。基于这一机制，压力的变化能够精确地映射到频率的变化上，从而实现无线且无源的压力测量。通过利用超材料固有的共振辐射来实现耦合读数，传感器集成的复杂性得到了显著降低，其在高压、高温和强电磁干扰环境中的工作可靠性也得到了提高。在设计阶段，通过有限元耦合模拟分析了超材料几何参数及其他因素对共振性能和压力灵敏度的影响规律。实验验证表明，该传感器在0—500 kPa范围内表现出出色的线性压力响应，并在高压区域保持良好的重复性和频率稳定性。最大灵敏度达到135 kHz/kPa，且在多次加载-卸载循环中频率漂移极小，充分证明了该设计的结构强度和可靠性满足工程要求。本研究中提出的传感器能够在航空航天发动机舱、高温冶金炉、深井压力监测、石油化工高腐蚀管道以及极端环境设备中实现长期稳定运行。这项研究不仅展示了将超材料与先进陶瓷工艺相结合以构建无线被动传感器的潜力，而且还为在恶劣环境中微波传感技术的工程应用提供了新的设计思路和工艺路线。

关键词： 压力传感器；无线无源；高温共烧陶瓷；陶瓷工艺；微波；航空航天领域

引用格式： FENG Rui, QIAO Yi, WU Dongyang, et al. Metamaterial pressure sensor based on ceramic for harsh environments. Journal of Measurement Science and Instrumentation, 2025, 16(4): 603-611. DOI: 10.62756/jmsi.1674-8042.2025058